ARR Sept. 1941

NATIONAL ADVISORY COMMITTEE FOR AERONAUTICS

WARTIME REPORT

ORIGINALLY ISSUED
September 1941 as
Advance Restricted Report

CRITICAL SPEEDS AND PROFILE DRAG OF THE INBOARD SECTIONS OF A CONVENTIONAL PROPELLER

By Arvo A. Luoma

Langley Memorial Aeronautical Laboratory
Langley Field, Va.

NACA

WASHINGTON

L - 369

CRITICAL SPEEDS AND PROFILE DRAG OF THE INBOARD SECTIONS OF A CONVENTIONAL PROPELLER

By Arvo A. Luoma

SUMMARY

The section critical speeds and profile drags of the shank and hub sections of a 10-foot 3-inch diameter propeller (Pittsburgh Screw and Bolt drawing no. 614 Cc 15) used on a current liquid-cooled-engine pursuit type of airplane were determined from tests made in the 8-foot high-speed wind tunnel.

A full-scale wooden propeller blade was made with the twist of the blade removed so that all sections operated approximately from a common zero-lift position, and then was mounted vertically in the wind tunnel, steel end supports being used on both ends of the wooden blade to increase the strength and rigidity of the set-up.

Section critical speeds were obtained from maximum negative pressure measurements. The profile drags at five sections were obtained by static- and total-pressure surveys of the wakes of these sections and the use of Jones' equations modified to include compressibility effects. Section normal-force coefficients were determined for two blade sections from complete pressure-distribution measurements.

Serious adverse compressibility effects can be expected on the shank and hub sections at speeds of the order of 400 miles per hour with subsequent detrimental effects on propulsive efficiency. Suitable fairings to delay the formation of the compressibility shock on these sections are desirable.

INTRODUCTION

Until recently adverse compressibility effects on propeller drag were given consideration only for tip sections operating at high tip speeds. Cylinder drag tests (reference 1) and other unpublished cylinder drag data indicate that at speeds of 325 miles per hour and higher the compressibility effects on the shank and hub sections of conventional propellers assume sufficient importance to justify efforts to improve these sections aerodynamically. Increasing attention should be especially focused on the shank and hub sections of propellers used on pursuit and interceptor aircraft, particularly those having liquid-cooled engines and thin nose forms because of the large amount of the thick and nearly cylindrical sections of the propeller that may be exposed.

From data obtained in tests made in the propeller-research tunnel, where because of the low speeds (110 mph) compressibility effects on the shank and the hub sections can be neglected, improvement in propulsive efficiency of about 4 percent was obtained by the use of shank fairings on a conventional propeller. At speeds where compressibility effects are pronounced such increases in propulsive efficiency can be expected to be more marked.

The purpose of the present investigation was, primarily, to determine the critical speeds and the profile-drag coefficients of the shank and hub sections of a propeller (Pittsburgh Screw and Bolt drawing no. 614 Cc 15) used on a current liquid-cooled-engine pursuit airplane.

APPARATUS AND METHODS

The tests were made in the 8-foot high-speed wind tunnel, which is a single-return, circular-section, closed-throat tunnel having an air speed continuously controllable from about 75 miles per hour to more than 500 miles per hour.

A full-scale model of a propeller blade (Pittsburgh Screw and Bolt drawing no. 614 Cc 15) of modified Clark Y section as used on a current liquid-cooled-engine pursuit type of airplane was used in the tests. This model was constructed of wood and included the stations from the hub (12-inch station) to the 48-inch station. (See fig. 1.) Station numbers are the distances in inches from the center line of the crankshaft to the airfoil section. The thin sections beyond the 48-inch station were not included because the low strength of the wooden model required a special method for supporting the blade in the wind tunnel.

The twist of the blade was removed so that the sections operated approximately from a common zero-lift position. The angles of zero lift for the various sections were calculated by the method given in the appendix of reference 2 and checked by Munk's method for determining zero-lift angle (reference 3). Table I gives the relationship between α the angle of attack, and α_a the absolute angle of attack (based on calculated zero-lift position).

A total of 53 static-pressure orifices were located at five sections of the model, so that complete pressure-distribution measurements were obtained at the 18- and 30-inch stations and peak negative pressures at the 12-, 24-, and 36-inch stations. The model was mounted vertically in the wind tunnel (fig. 2) and steel end supports were used to prevent excessive deflection of the wooden blade. Provision was made for changing the absolute angle of attack from -1° to 13°.

Static-pressure measurements were made at velocities from 140 miles per hour to 360 miles per hour and the absolute angle of attack was varied from -1° to 12°. Simultaneous observations of the pressures acting at the orifices were obtained by photographing a multiple-tube manometer in which tetrabromoethane (specific gravity approximately 3) was used.

The profile drags at five sections were obtained by the momentum method and the use of Jones' equations (reference 4) modified to include compressibility effects. Several angles of attack were included and velocities from 140 miles per hour to 360 miles per hour were covered. Simultaneous observations of the total-head and static pressure distribution behind the propeller sections were made by photographing a multiple-tube integrating manometer in which alcohol was used.

PRECISION

The critical speeds of the propeller sections were determined from static pressure measurements, and it is estimated that the critical Mach numbers are accurate to within ± 0.02.

The accuracy of the profile drags for the 24-inch station (0.241 thickness ratio) and the thinner sections can be considered equal to that usually obtained by the momentum method. For the 12-inch station (0.977 thickness ratio) and the 18-inch station (0.451 thickness ratio) the possible error in drag is probably greater because the bluffness and the turbulent nature of the flow in the wake of these sections undoubtedly have some effect on the results.

In the derivation of Jones' equations for drag determination by the momentum method, the flow of air behind a body is assumed to be negligibly inclined to its original direction, but, if the body is bluff and the total- and static-pressure tubes are located close behind the body, a source of error may be introduced since in this case the assumption of negligible inclination of the flow at the measuring plane may no longer be valid. On the other hand, with a body of varying thickness ratio like the propeller blade tested, there is probably sufficient mixing and cross flow of the air behind the blade to defeat efforts to measure the profile drag of a particular section by locating the pressure tubes any great distance aft of this section. In view of these facts, the total- and static-pressure surveys were made at distances behind the trailing edges of the sections as follows: 1.6 chord lengths behind the 12-inch station, 0.9 chord length behind the 18-inch station, 1.5 chord lengths behind the 24-inch station, and 1.3 chord lengths behind the 30-inch and 36-inch stations.

Systematic errors due to buoyancy and constriction effects were negligible.

RESULTS AND DISCUSSION

The symbols used in this report are defined as follows:

α angle of attack

α_a angle of attack, absolute (measured from calculated zero-lift position)

c_{d_o} section profile-drag coefficient

c_n section normal-force coefficient

c_l section lift coefficient

V velocity

p static pressure

ρ mass density

a speed of sound

q dynamic pressure $(1/2\ \rho_o V_o^2)$

P pressure coefficient $\left(\frac{p-p_o}{q_o}\right)$

M Mach number (V_o/a)

h maximum thickness of airfoil section

b chord of section

μ coefficient of viscosity

R Reynolds number $\left(\frac{V_o \rho_o b}{\mu_o}\right)$

x distance along chord from leading edge

r radial distance from axis of rotation of propeller to a blade section

R radial distance from axis of rotation of propeller to tip of propeller

n revolutions per unit time of propeller

V_r resultant velocity of propeller blade section

Subscripts:

O values in the undisturbed stream

cr values when the local speed of sound has been reached at some point on the airfoil section

The critical Mach numbers of the shank and hub sections were determined from the intersection of the curves of P_{max} against M and the P_{cr} curve, as shown in figures 3 to 7. Where tests were limited because of high loads, the curves of P_{max} against M were extrapolated through higher Mach number ranges. The extrapolations are believed accurate except possibly at high lift coefficients where separation effects may be encountered. The consequent errors in determining M_{cr}, however, tend to be small because the variation of the P_{cr} curve in this Mach number range is such that a given change in P produces a relatively small change in M_{cr}. (Note P_{cr} curve in figs. 3 to 7. See also equations (6a) and (6b) of reference 5.) Table II gives estimated and experimental values of M_{cr} and shows the good agreement between theory and experiment. The estimated values of M_{cr} were obtained by increasing computed maximum negative pressure coefficients for incompressible flow or experimentally determined maximum negative pressure coefficients at low speed by the factor $1/\sqrt{1 - M^2}$. (See equation (7) of reference 5.)

The data of figures 3 to 7 illustrate the variation of P_{max} with Mach number, and it is seen that the variation at low values of P_{max} is regular though somewhat greater than theory indicates. Figures 4 to 7 reveal the fact that at high values of P_{max} there is a tendency for P_{max} to increase at low Mach numbers. The probable reason for this is that the adverse pressure gradient over the upper surface of a section becomes sufficiently bad, owing to induced compressibility effects so that separation occurs on this surface. As a consequence, there is a drop in peak negative pressures as the Mach number is increased from its lowest value to somewhat higher values corresponding to the movement of the separation point to its farthest forward position. The erratic behavior of the pressure peaks of the 97.7-percent-thick 12-inch station as illustrated in figure 3 can probably be explained partly by the foregoing reasoning and partly by the fact that the section was operating near the critical Reynolds number.

Figure 8 gives experimental and theoretical pressure distributions at several lift coefficients for the 15.3-percent-thick 30-inch station. The closeness of the agreement is indicative of the accuracy with which M_{cr} can be theoretically calculated.

The variation of M_{cr} with radius and thickness ratio is shown in figures 9 and 10, the variation with h/b being particularly well brought out. The curves illustrate the fact that the M_{cr} of the nearly cylindrical hub section is independent of angle of attack and that the critical speeds of the sections become more dependent on angle of attack as the thickness ratio decreases. The curves also show that at zero lift coefficient and at low lift coefficients shock occurs first on the lower surface of some of the sections before it occurs on the upper surface.

Curves of M_{cr} against α_a for the 10-percent-thick section are shown in figure 11, the data for these curves being taken from the curves of figure 10. For comparison purposes M_{cr} values for a 10-percent-thick Clark Y section as determined from section force test data (reference 6) are included, as well as theoretical values for 10-percent-thick Clark Y and Clark YM sections (data from reference 5). As can be seen, the M_{cr} values for the propeller section are uniformly somewhat lower than the reference values for those angles of attack where compressibility shock first appears on the upper surface of the section. The main significance of figure 11, however, is that, with this type of section, attempts to relieve tip critical-speed difficulties by decreasing the c_l of the tip sections (wash-out of tip) are limited by the establishment of lower surface shock for lift coefficients less than approximately 0.2.

Curves of relative wind velocity V_r against radius ratio r/R are shown in figure 12 for assumed airplane speeds of 400 miles per hour for maximum speed and 325 miles per hour for cruising speed. A constant-speed propeller of 1500 rpm was used in the calculation of the data for these curves. Also included are the experimentally determined critical speeds of the propeller sections for $\alpha_a = 4^{\circ}$ and $\alpha_a = 2^{\circ}$ for sea-level conditions. The section lift coefficients of the 12-, 18-, and 30-inch stations are indicated on these critical-speed curves. On the curve at $\alpha_a = 2^{\circ}$ for r/R values outboard of 0.46, shock occurs first on the lower surface. The additional curves shown are theoretical critical-speed curves for sea-level conditions, and were determined: (1) from theoretical pressure distributions made for four sections of the propeller at lift coefficients of 0.4 and 0.2, and (2) from the data of reference 5 for a Clark Y section which had the same thickness ratio as the propeller sections for equal values of r/R. From figure 12 it is evident that for the assumed maximum speed at sea-level conditions pronounced compressibility effects should be expected. At altitude these adverse effects are worse, that is, the critical speeds of the sections are lower. It is not to be inferred, however, that the general problem is as serious as indicated here. This particular airplane-engine-propeller combination as originally built suffered materially because of improper gear ratio. Provision of a lower speed gear can help materially and studies have indicated that clearance from adverse compressibility effects may be possible at speeds approaching 400 miles per hour. Beyond this speed material increases in solidity will likely be required.

The shank fairings used in the propeller-research-tunnel tests, which resulted in an increase of propulsive efficiency of 4 percent at low speed, were of 40-percent thickness ratio at the 12-inch station. A 25-percent thick fairing section at the 12-inch station could be expected to account for even greater increases in propulsive efficiency, particularly at higher speeds.

Section normal-force coefficients determined from complete pressure-distribution data for the 18-inch station (0.451 thickness ratio) and the 30-inch station (0.153 thickness ratio) are illustrated by figures 13 and 14. The variation of the slope of the c_n curve of the 18-inch station with Mach number is entirely unlike the theoretical variation whereby the slope increases with Mach number for speeds up to the critical speed. Owing to the thickness of this section, marked separation effects are induced as M is increased, affecting thereby the forces acting on the section. In figure 14 the data for the 30-inch station indicate some increase in slope with Mach number. The c_n values for the lowest Mach number are somewhat erratic, as are also the values at $\alpha_a = 10^\circ$ and $\alpha_a = 12^\circ$. From an examination of the pressure-distribution plots, the high c_n value for $\alpha_a = 0^\circ$ and $M = 0.185$ is seen to be due to the influence of the pressures on the lower surface of this section. These pressures are sufficiently more positive at the lowest Mach number to counterbalance the inclination of c_n to increase, owing to induced compressibility effects at higher Mach numbers. At high angles there is a tendency for the pressures on the upper surface aft of the 0.65 chord station to become more negative at low Mach numbers, so that as a consequence the c_n values tend to be higher at low Mach numbers.

The profile drag of the shank and hub sections was determined from total- and static-pressure surveys of the wakes of the sections, due account being taken of compressibility effects in the computing equations used. Figures 15 and 16 give the profile drag of the 97.7-percent thick 12-inch station. For comparison, the drag of a 4-inch diameter cylinder as obtained from unpublished tests made in the 8-foot high-speed tunnel is included. From figures 15 and 16 and the pressure curves of figure 3, it is evident that the 12-inch station section was operating near the critical Reynolds number region where the flow, as a result of the building up of turbulence in the boundary layer, changes from laminar separation ahead of the central plane to turbulent separation aft of the central plane. This change in flow has an appreciable effect on the pressure distribution about the section (particularly the maximum negative pressures and the pressures aft of the position of the maximum negative pressures) and the profile drag of the section.

A probable explanation for the behavior of the profile drag of the 45.1-percent thick 18-inch station shown in figure 17 for several angles of attack is as follows: At the lowest Reynolds number (690,000) the flow was laminar with laminar separation somewhere aft of the maximum thickness; with increasing Reynolds number the point of separation moved forward with a resulting increase in wake width and hence a larger drag; and, with further increase in Reynolds number, transition from laminar boundary layer to turbulent boundary layer took place ahead of the separation point, with a resulting turbulent separation farther aft on the chord than when the separation was laminar, and as a consequence a smaller wake width and a decrease in drag resulted. Hence, with increase in Reynolds number, the initial increase in drag and then the decrease occurs.

Figure 18 gives the profile drag of the 24.1-percent thick 24-inch station for several angles of attack. At $\alpha_a = 0^\circ$ separation effects similar to those obtained for the thicker 18-inch station appear. In this instance the disturbances are probably connected with the lower surface only. At high angles of attack the marked rise in drag is probably due to separation effects induced by compressibility.

The profile drags of the 30-inch and 36-inch stations are shown in figures 19 and 20 for several different angles of attack. The general similarity to section data is to be noted, and the order of magnitude is about the same as section data for these Reynolds numbers.

CONCLUSIONS

The results indicate that serious adverse compressibility effects can be expected at speeds of the order of 400 miles per hour.

It is evident that suitable fairings for the shank and hub sections are a necessity for maximum propulsive efficiency.

Good agreement in critical speed between basic section data and the values obtained from the sections as used in a propeller can be expected for the inboard stations.

Langley Memorial Aeronautical Laboratory,
National Advisory Committee for Aeronautics,
Langley Field, Va.

REFERENCES

1. Lindsey, W. F.: Drag of Cylinders of Simple Shapes. Rep. No. 619, NACA, 1938.

2. Jacobs, Eastman N., Ward, Kenneth E., and Pinkerton, Robert M.: The Characteristics of 78 Related Airfoil Sections from Tests in the Variable-Density Wind Tunnel. Rep. No. 460, NACA, 1933.

3. Munk, Max M.: Fundamentals of Fluid Dynamics for Aircraft Designers. The Ronald Press Co., 1929, p. 80.

4. The Cambridge University Aeronautics Laboratory: The Measurement of Profile Drag by the Pitot-Traverse Method. R. & M. No. 1688, British A.R.C., 1936.

5. Robinson, Russell G., and Wright, Ray H.: Estimation of Critical Speeds of Airfoils and Streamline Bodies. NACA confidential rep., 1940.

6. Stack, John: The N.A.C.A. High-Speed Wind Tunnel and Tests of Six Propeller Sections. Rep. No. 463, NACA, 1933.

TABLE I.- THE ANGLE OF ATTACK α OF THE VARIOUS SECTIONS CORRESPONDING TO THE ANGLE α_a

Section (in.)	β (deg)
12	0
18	-1.2
24	-2.9
30	-4.0
36	-4.4
42	-3.6
48	-3.2

$\alpha = \beta + \alpha_a$

α_a (deg)	α (deg)						
	12-in.	18-in.	24-in.	30-in.	36-in.	42-in.	48-in.
-1	-1	-2.2	-3.9	-5.0	-5.4	-4.6	-4.2
0	0	-1.2	-2.9	-4.0	-4.4	-3.6	-3.2
2	2	.8	-.9	-2.0	-2.4	-1.6	-1.2
4	4	2.8	1.1	0	-.4	.4	.8
6	6	4.8	3.1	2.0	1.6	2.4	2.8
8	8	6.8	5.1	4.0	3.6	4.4	4.8
10	10	8.8	7.1	6.0	5.6	6.4	6.8
12	12	10.8	9.1	8.0	7.6	8.4	8.8

TABLE [illegible]. COMPARISON OF EXPERIMENTALLY DETERMINED CRITICAL MACH NUMBERS WITH ESTIMATED VALUES FOR BLADE SECTIONS

Station (in)	Surface	$\alpha_a = -1^\circ$		$\alpha_a = 0^\circ$		$\alpha_a = 2^\circ$		$\alpha_a = 4^\circ$		$\alpha_a = 6^\circ$		$\alpha_a = 8^\circ$		$\alpha_a = 10^\circ$		$\alpha_a = 12^\circ$	
		Estimated	Experimental	Estimated	Experimental	Estimated	Experimental	Estimated	Experimental	Estimated	Experimental	Estimated	Experimental	Estimated	Experimental	Estimated	Experimental
12	Upper	---	---	0.45	0.46	0.45	0.45	0.45	0.46	0.45	0.45	0.46	0.46	0.46	0.45	0.46	0.45
	Lower	---	---	---	.46	---	.48	---	.50		.50		.50		.49		.48
18	Upper	0.56	0.56	.56	.55	.55	.54	.53	.52	.52	.51	.51	.50	.49	.48	.48	.47
	Lower	.57	.57	.59	.58	.59	.60		.58								
24	Upper	.64	.63	.64	.62	.63	.60	.60	.58	.57	.56	.55	.53	.52	.51	.49	.49
	Lower	.60	.61	.64	.64	.71	.68		.69								
30	Upper	.71	.68	[a] .70/.72	.66	[a] .66/.68	.65	[a] .61/.64	.62	.58	.58	.56	.55	.52	.51	.50	.48
	Lower	.51	.50	[a] .53/.52	.52	[a] .61/.60	.62	[a] .72/.70	.70								
36	Upper	.74	.70	[a] .71/.74	.68	[a] .69/.71	.67	[a] .64/.66	.635	.60	.60	.56	.56	.51	.50	.48	.46
	Lower	.53	.52	[a] .56/.57	.55	[a] .66/.67	.645	[a] —/.82	.67								
42	Upper			[a] —/.77		[a] —/.73		[a] —/.68									
	Lower			[a] —/.60		[a] —/.71		[a] —/.90									
48	Upper			[a] —/.78		[a] —/.74		[a] —/.68									
	Lower			[a] —/.62		[a] —/.75		[a] —/.97									

[a]Estimated values were determined from negative P_{max} values from theoretical incompressible pressure distributions and increased by factor $1/\sqrt{1 - M_2}$. Other estimated values were determined from low-speed experimentally obtained negative P_{max} values increased by factor $1/\sqrt{1 - M^2}$.

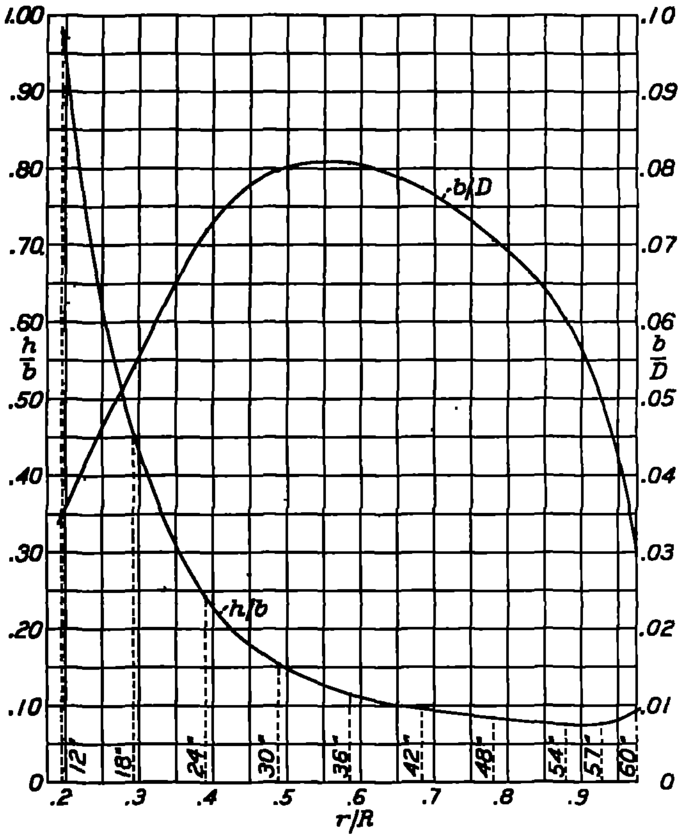

Figure 1.- Blade-form curve for steel propeller 10 feet 3 inches in diameter. Pittsburgh Screw and Bolt drawing no. 614Co15.

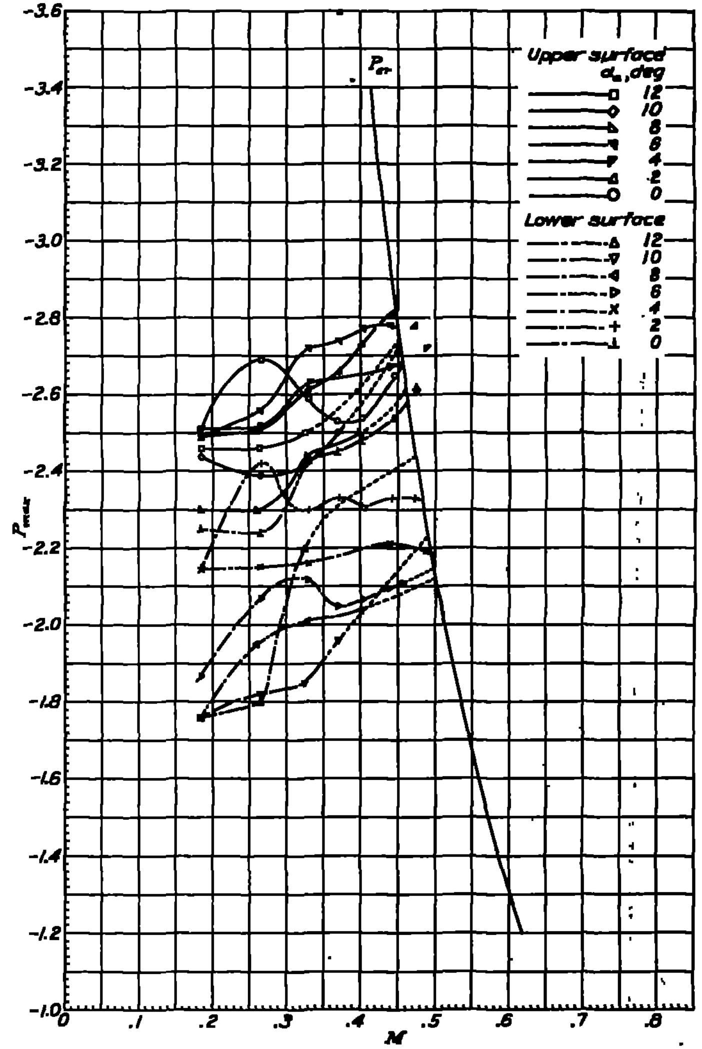

Figure 3.- Effect of compressibility on the maximum negative pressure coefficient for the 12-inch station.

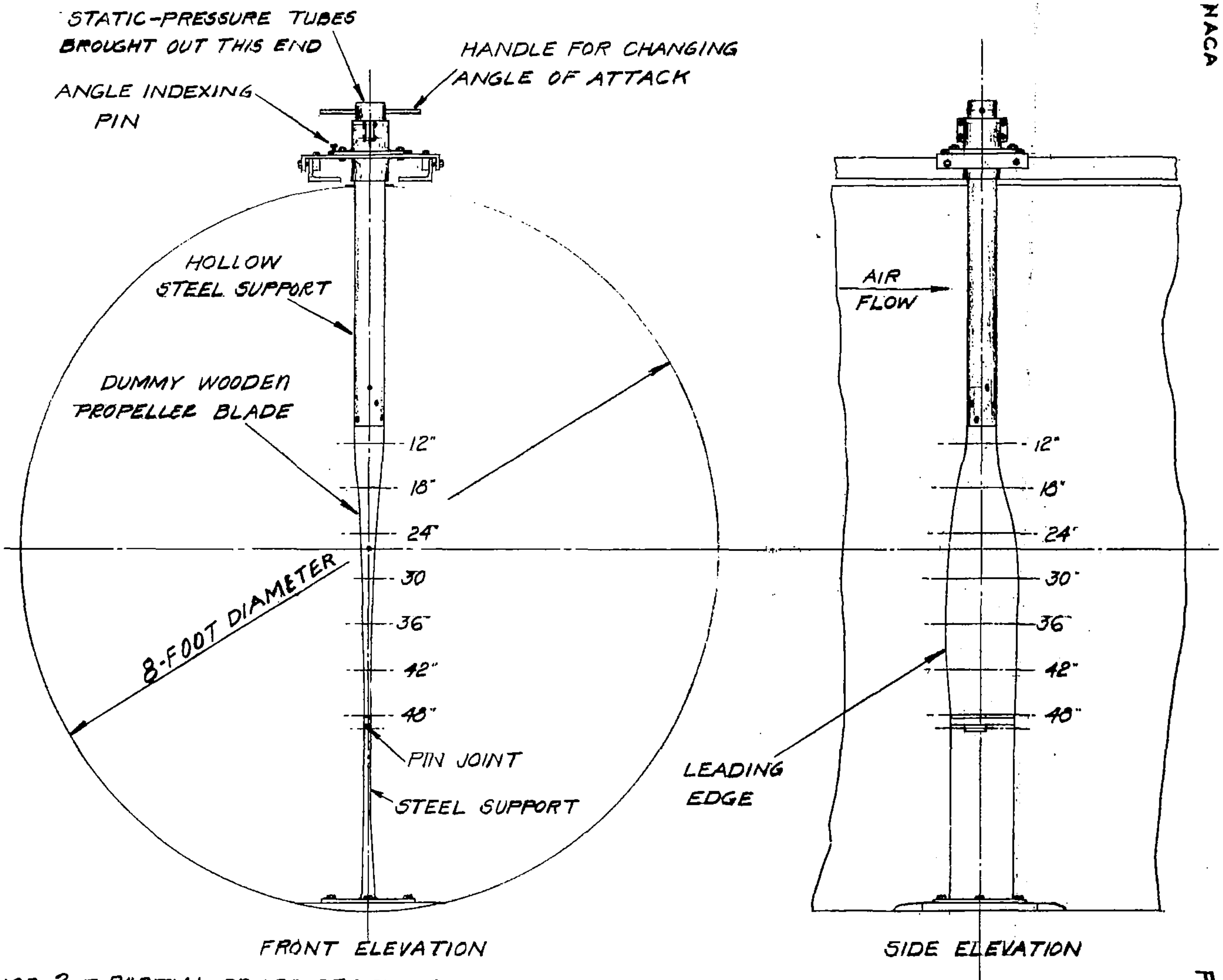

FIGURE 2.– PARTIAL CROSS SECTIONS OF TUNNEL SHOWING DUMMY PROPELLER BLADE AND METHOD OF SUPPORT

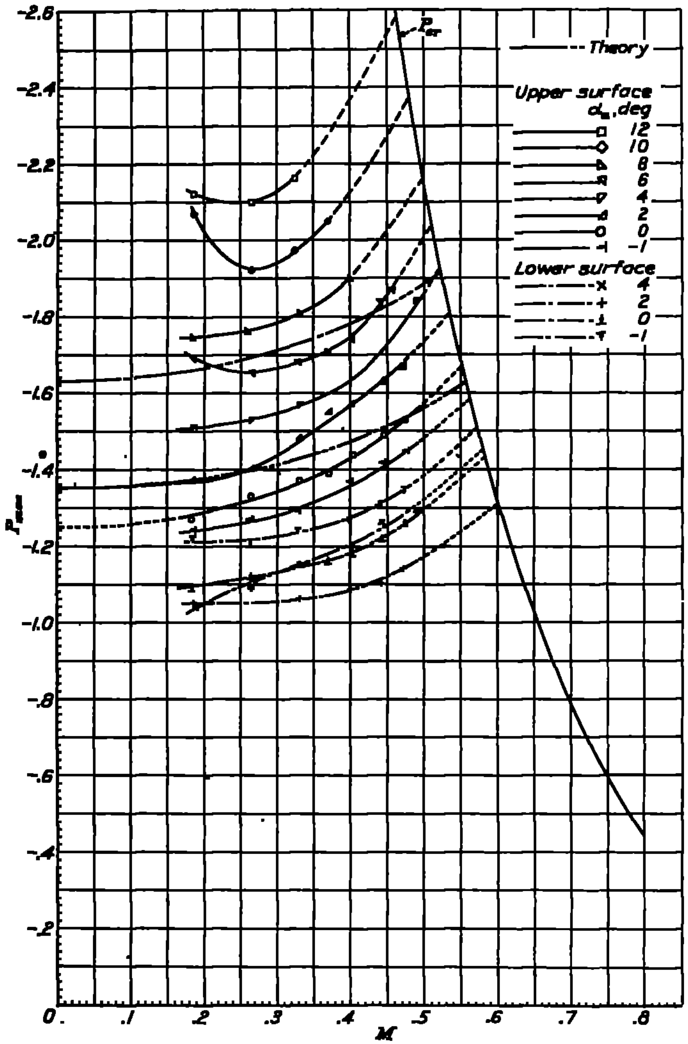

Figure 4.- For the 18-inch station.

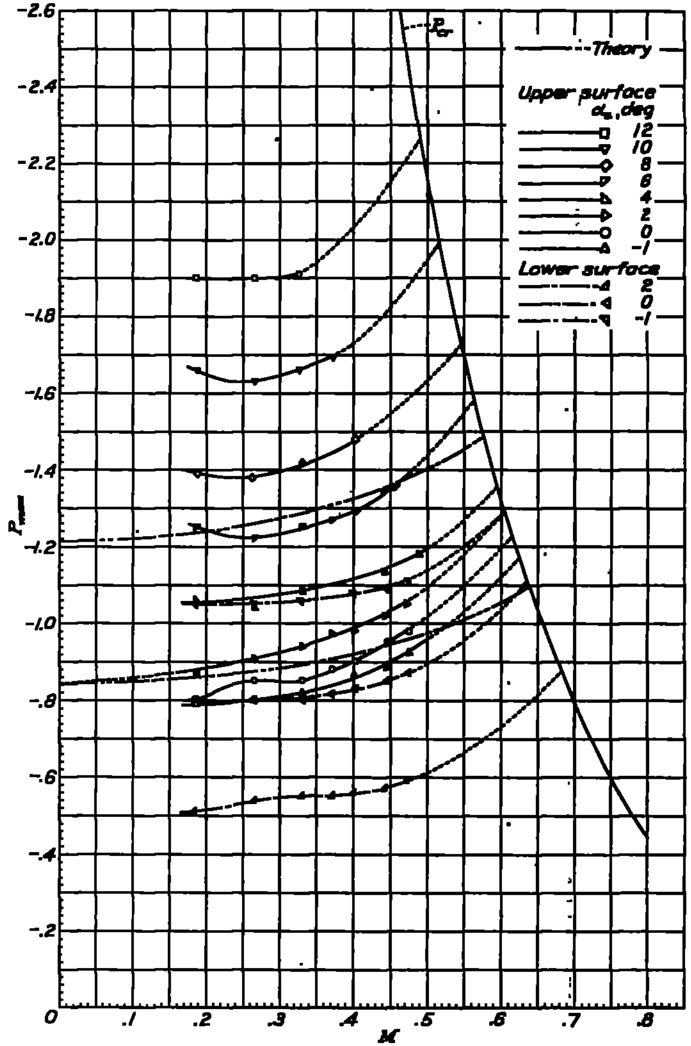

Figure 5.- For the 24-inch station.

Figure 4,5.- Effect of compressibility on the maximum negative pressure coefficient for the 18 and 24-inch stations.

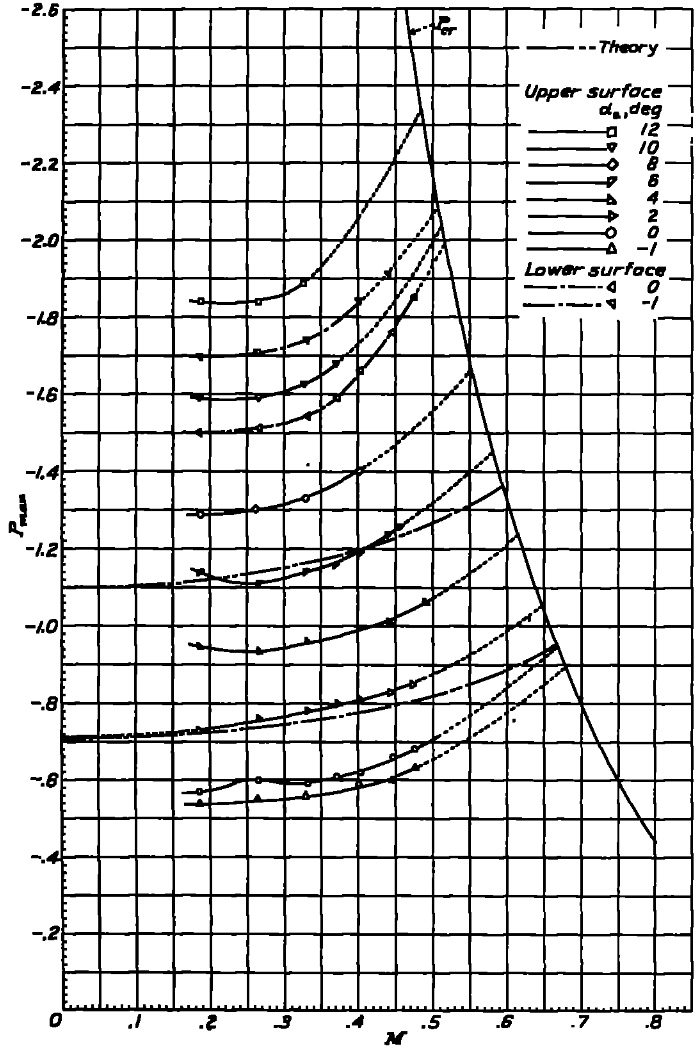

Figure 6.- For the 30-inch station.

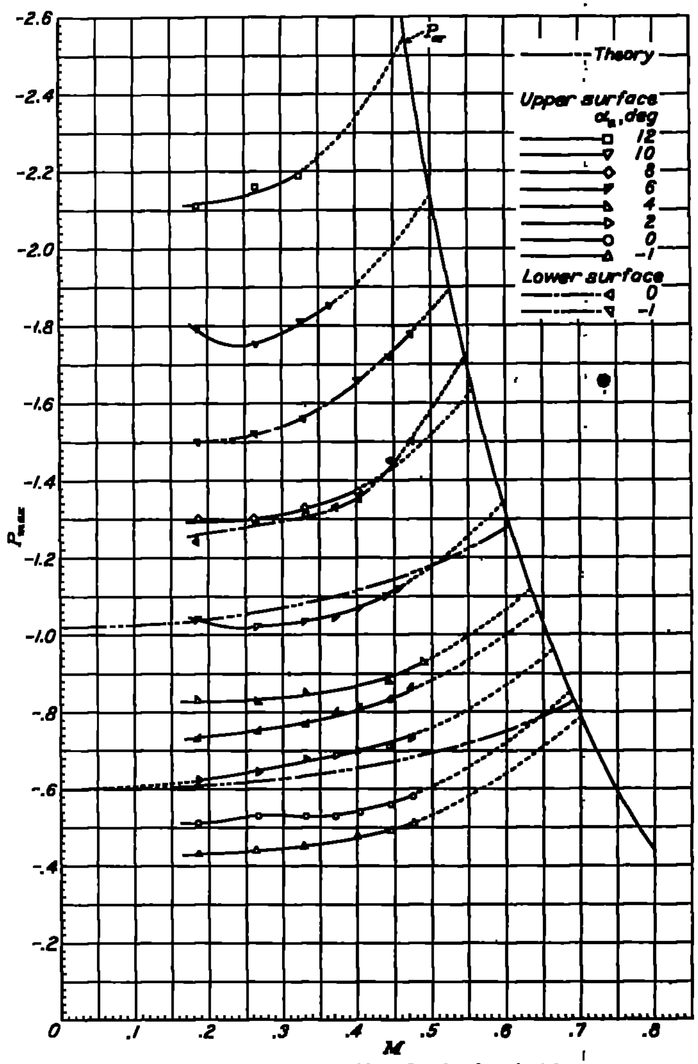

Figure 7.- For the 36-inch station.

Figures 6,7.- Effect of compressibility on the maximum negative pressure coefficient for the 30 and 36-inch stations.

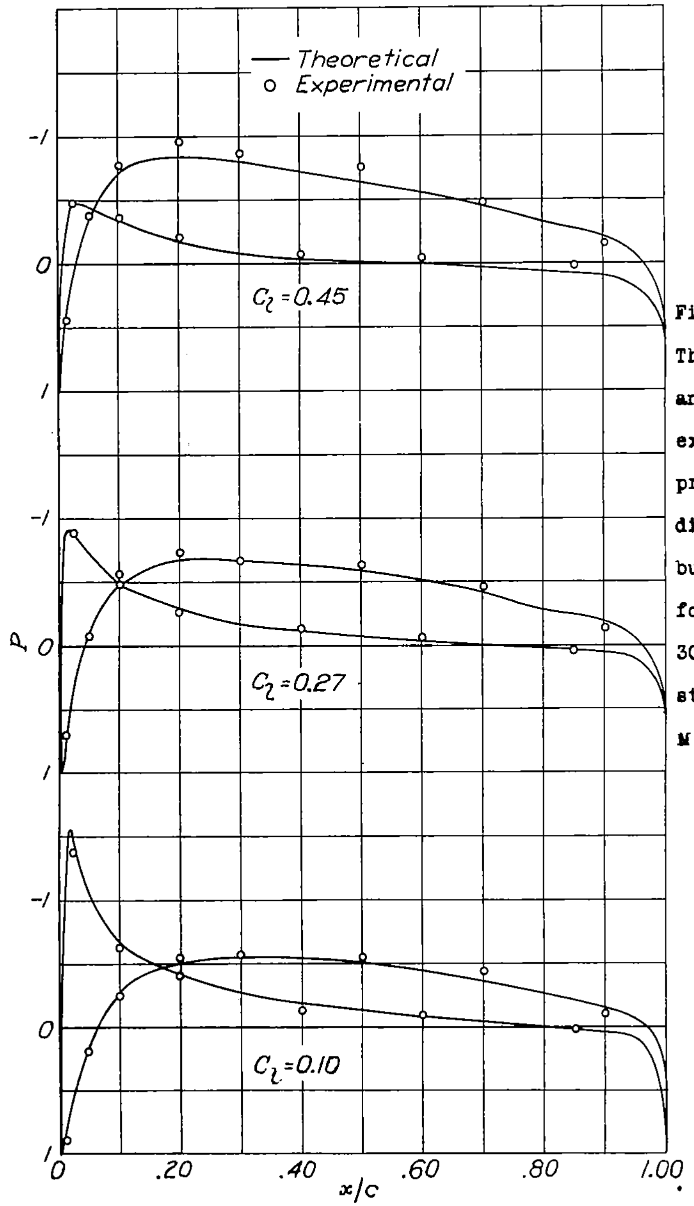

Figure 8.- Theoretical and experimental pressure distributions for the 30-inch station. M = 0.185

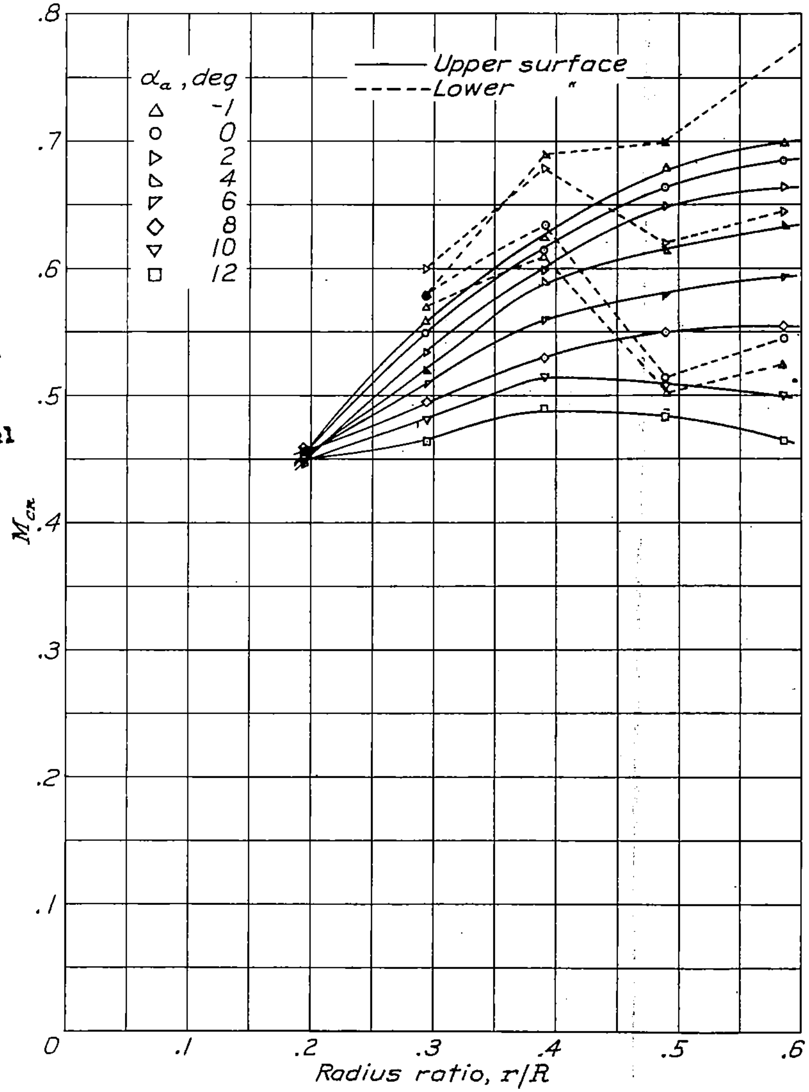

Figure 9.- Experimental critical Mach numbers for blade stations given in terms of radius ratio.

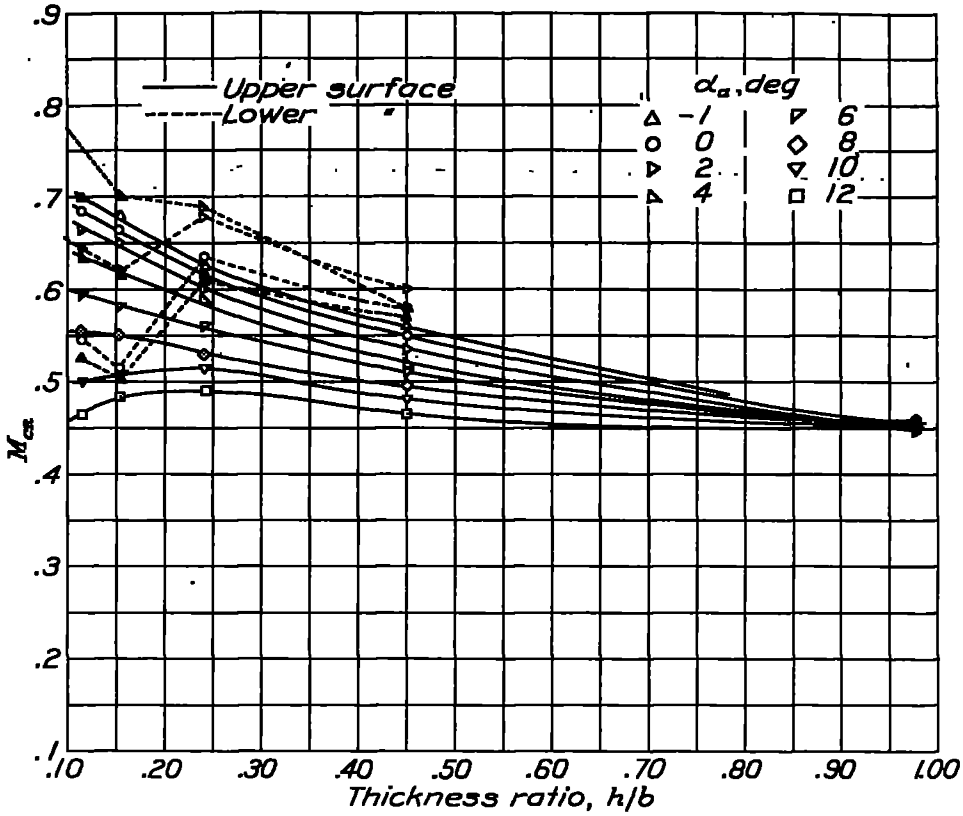

Figure 10.- Experimental critical Mach numbers for blade stations given in terms of thickness ratio.

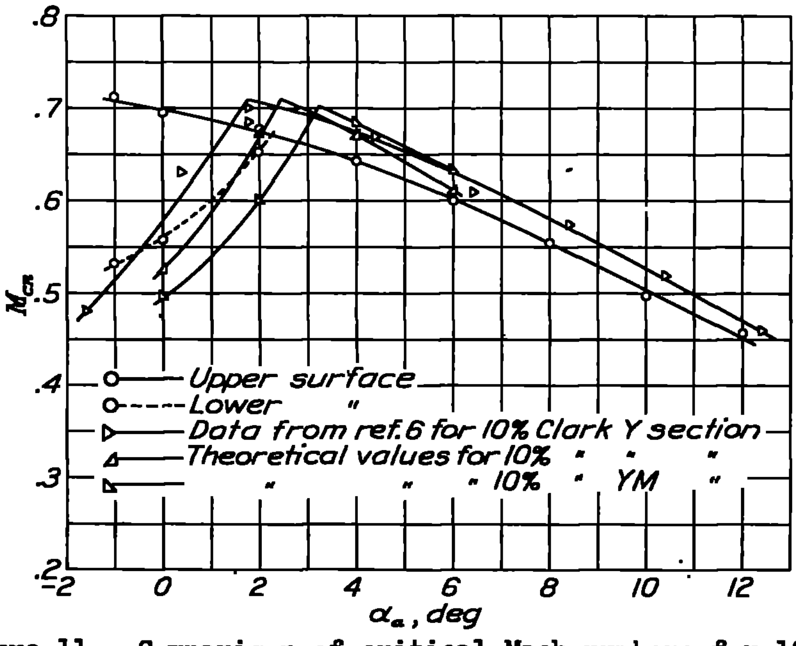

Figure 11.- Comparison of critical Mach numbers for 10-percent-thick sections.

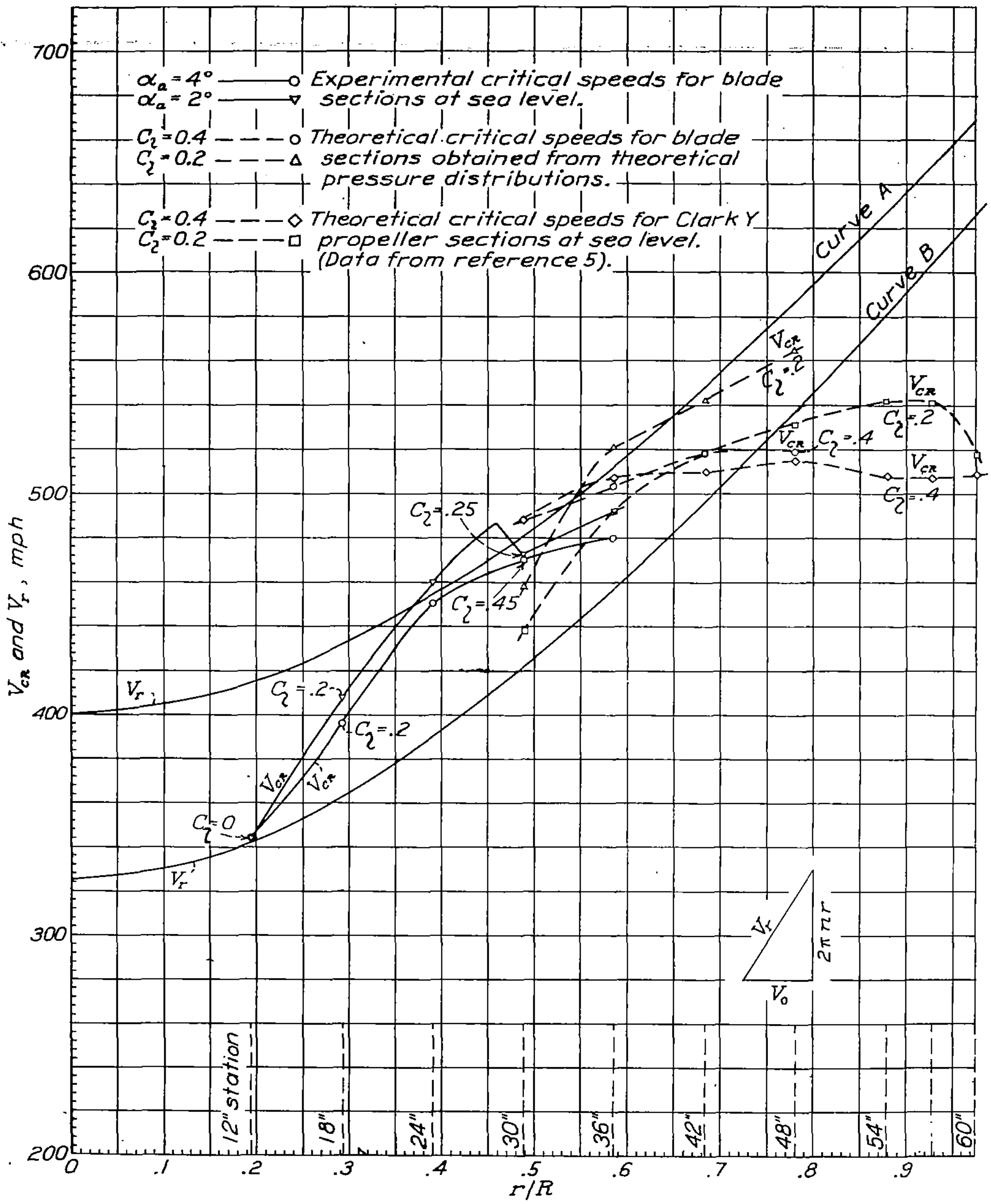

Figure 12.- Comparison of blade section operating speeds and critical speeds. Curve A, V_r **against r/R** for an assumed maximum airplane speed of 400 miles per hour and a propeller speed of 1500 rpm. Curve B, V_r against r/R for an assumed cruising speed of 325 miles per hour and a propeller speed of 1500 rpm.

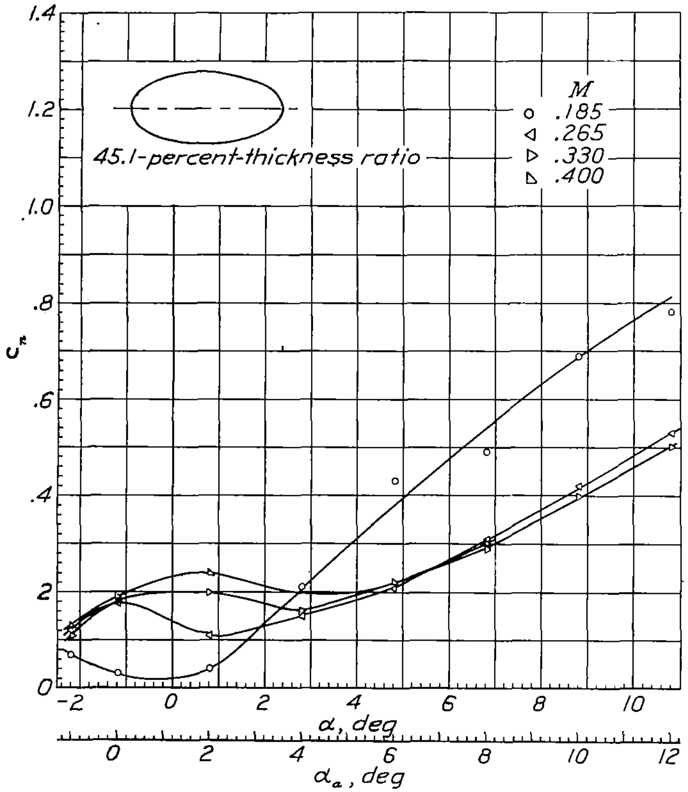

Figure 13.- 18-inch station.

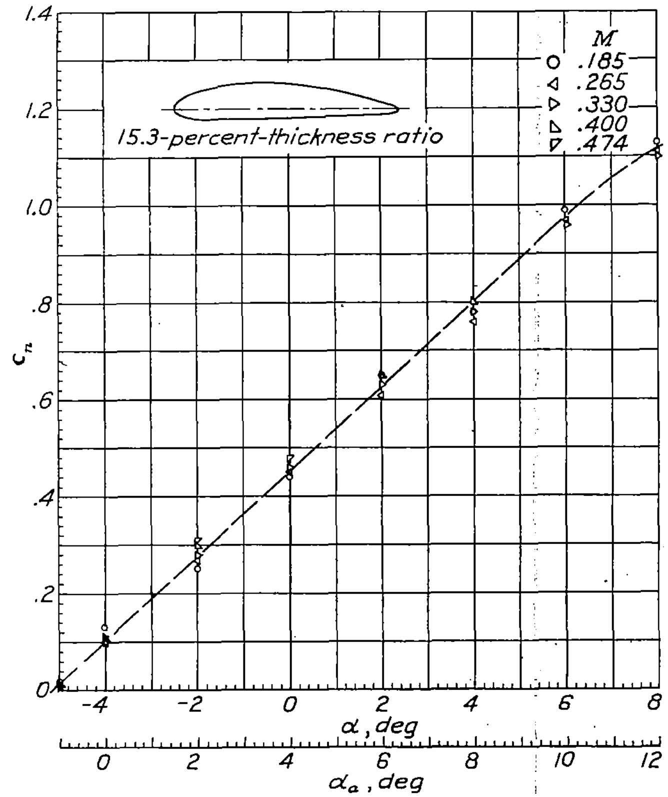

Figure 14.- 30-inch station.

Figures 13,14.- Section normal-force coefficient characteristics for various Mach numbers; 18-inch and 30-inch stations.

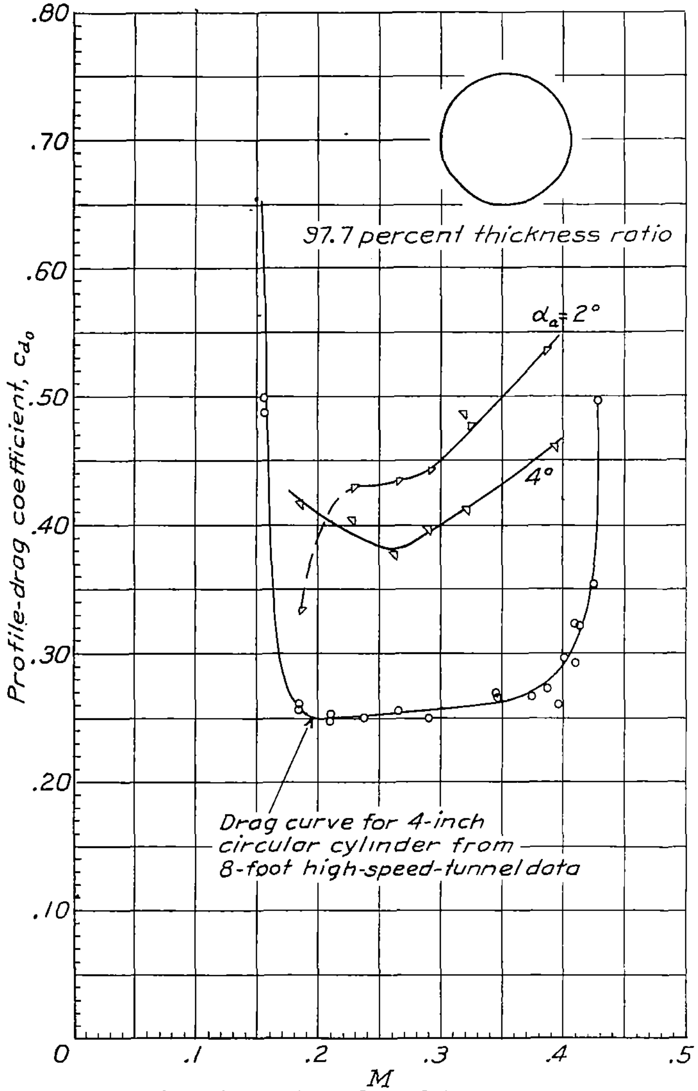

Figure 15.- Variation of profile drag coefficient with Mach number for 12-inch station.

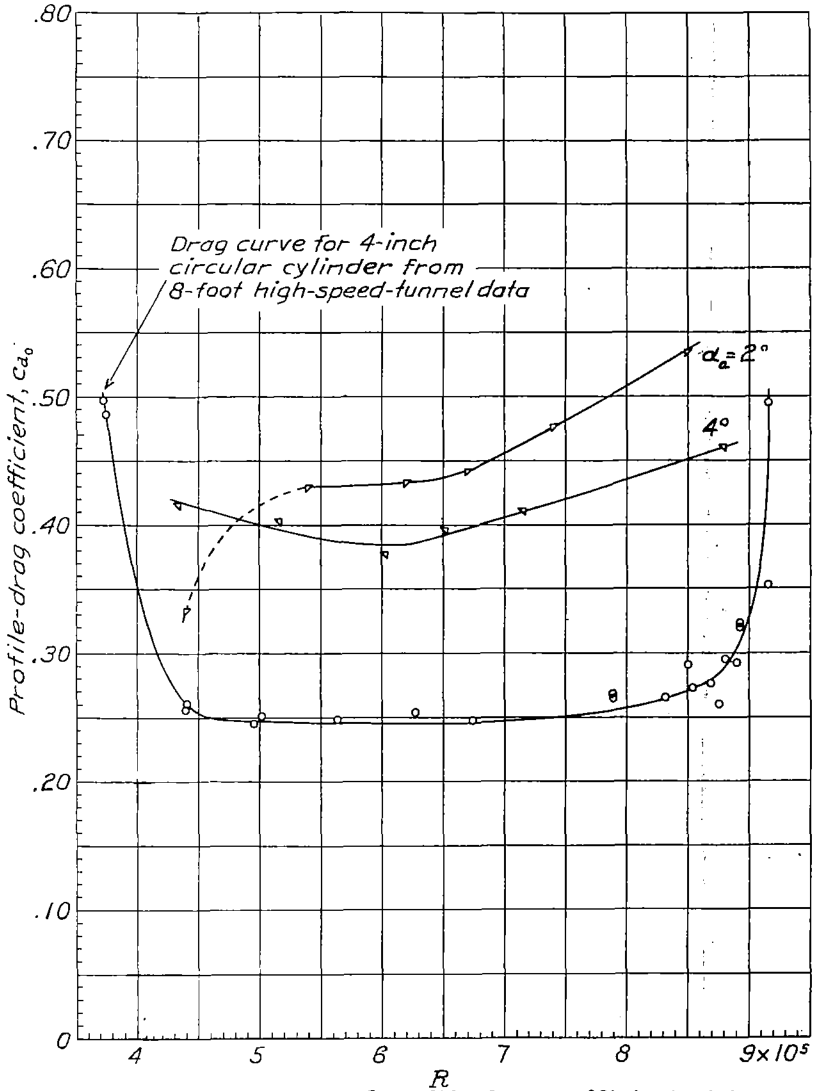

Figure 16.- Variation of profile drag coefficient with Reynolds number for 12-inch station.

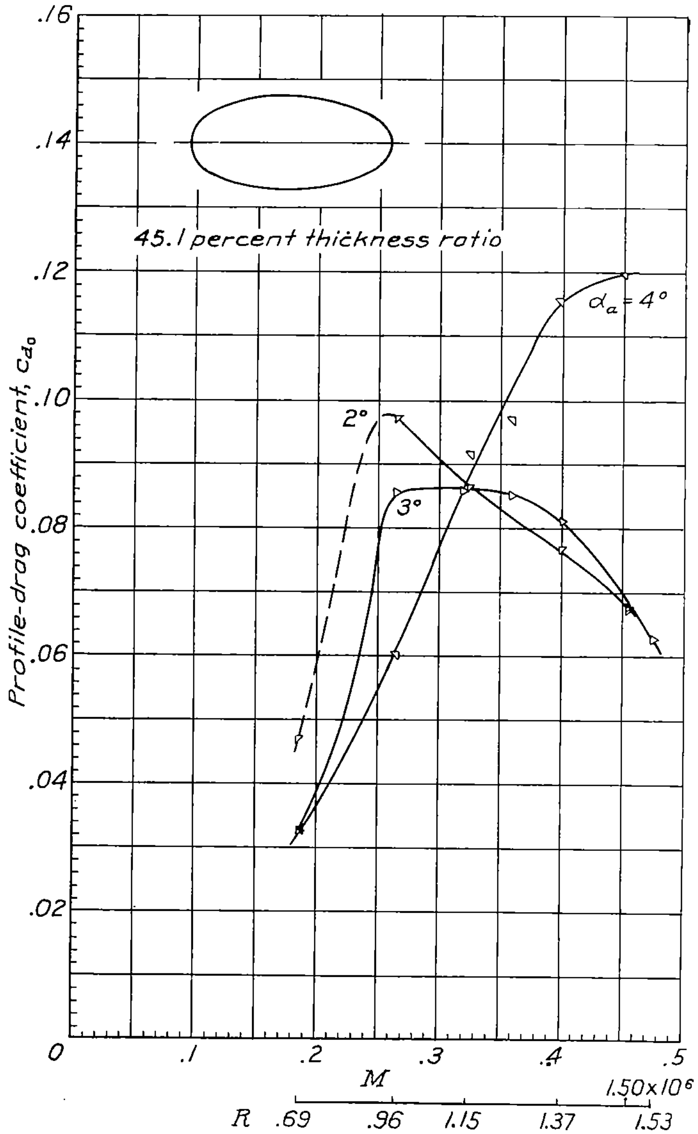

Figure 17.- Profile drag of 18-inch station.

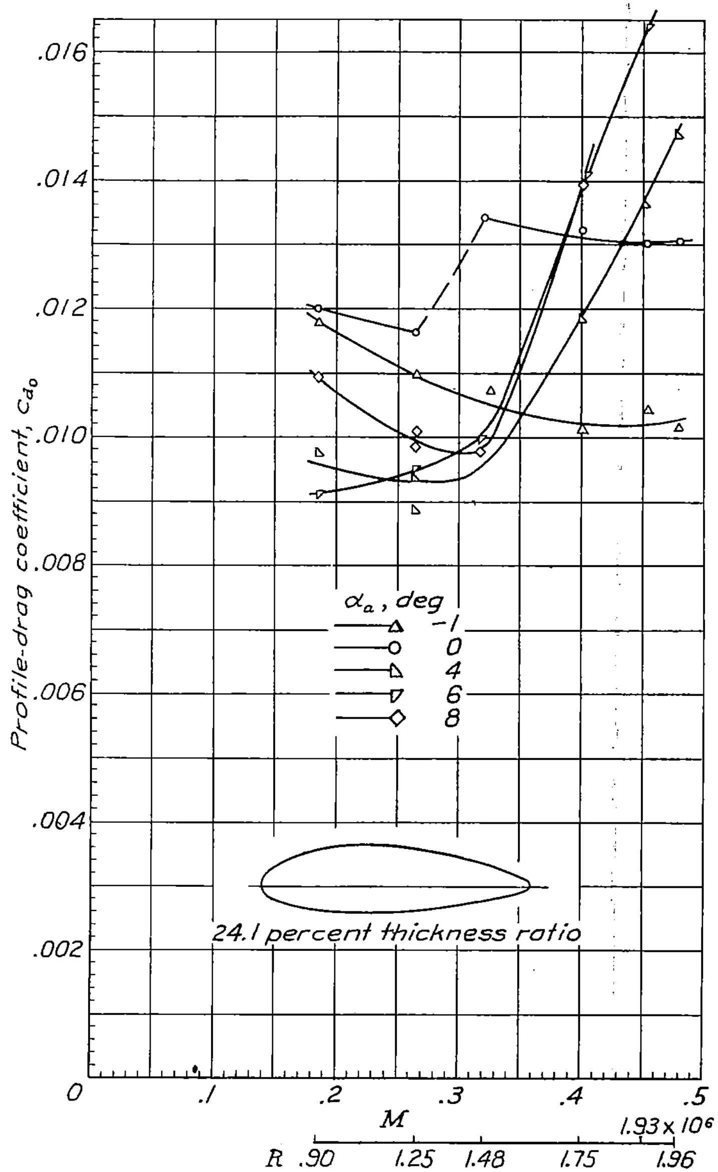

Figure 18.- Profile drag of 24-inch station.

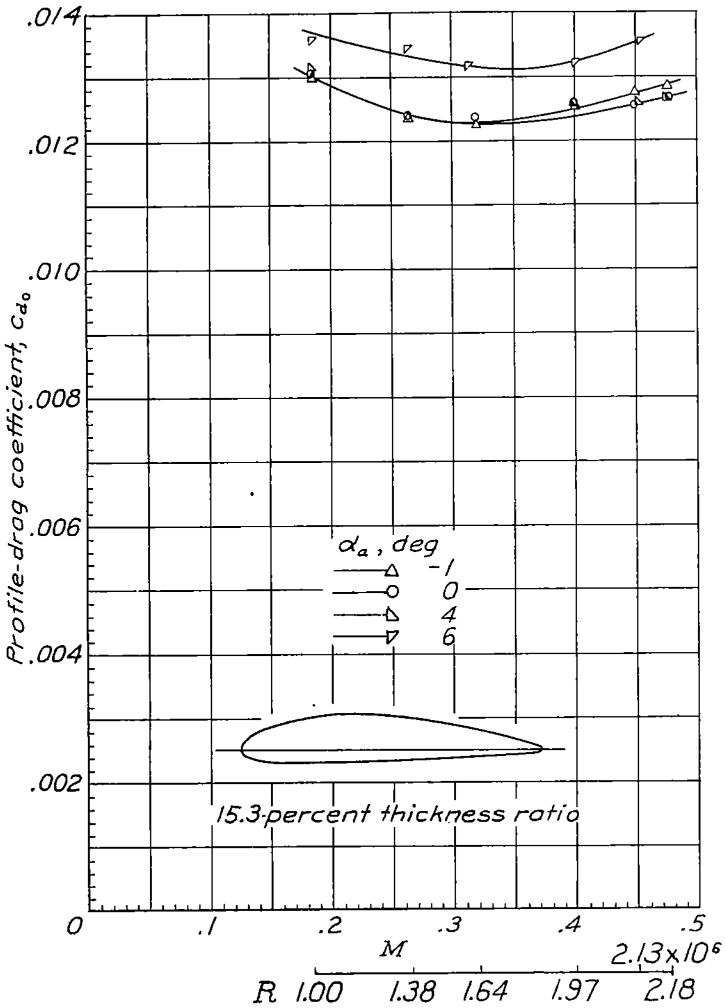

Figure 19.- Profile drag of 30-inch station.

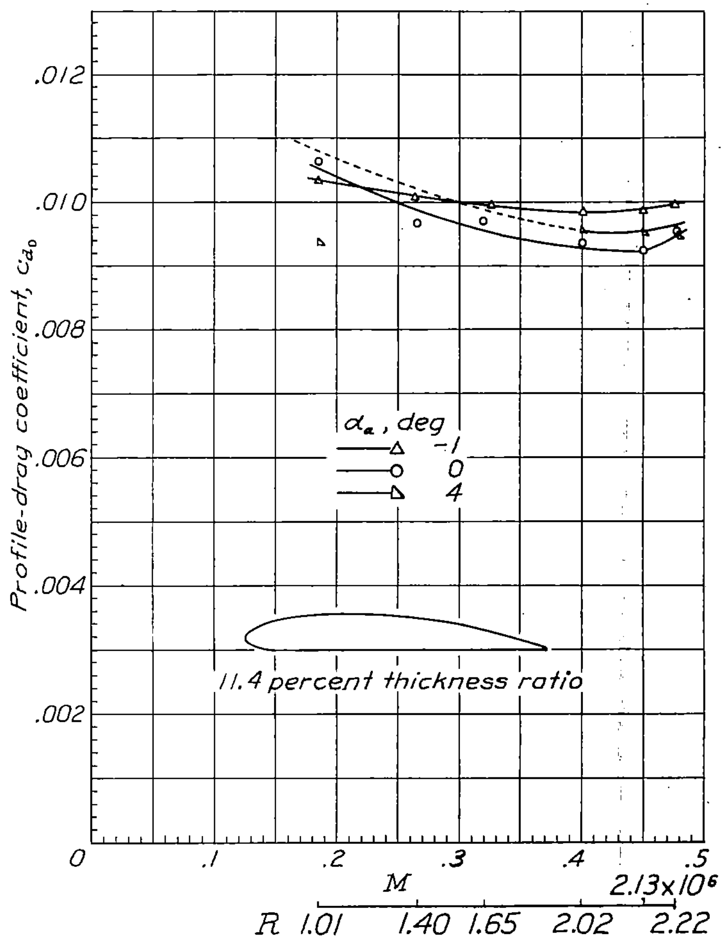

Figure 20.- Profile drag of 36-inch station.